Genome Instability and Pressure on Non-Homologous end Joining drives Chemotherapy Resistance via a DNA Repair Crisis Switch in Triple Negative Breast Cancer.

Adrian Wiegmans (adrian.wiegmans@qut.edu.au)
Queensland University of Technology https://orcid.org/0000-0003-4059-5988
Ambber Ward
QIMR Berghofer: QIMR Berghofer Medical Research Institute
Ekaterina Ivanova
Queensland University of Technology
Pascal H G Duijf
Queensland University of Technology
Romy VanOosterhout
QIMR: QIMR Berghofer Medical Research Institute
Martin C Sadowski
Queensland University of Technology
Greg Kelly
QIMR: QIMR Berghofer Medical Research Institute
Scott Morrical
University of Vermont College of Medicine
Jason S Lee
QIMR Berghofer: QIMR Berghofer Medical Research Institute
Derek J Richard
Queensland University of Technology

Research

Keywords: Chemoresistance, RAD51, triple negative breast cancer, prognostic, genome instability

Posted Date: November 12th, 2020

DOI: https://doi.org/10.21203/rs.3.rs-103661/v1

Version of Record: A version of this preprint was published at NAR Cancer on April 9th, 2021. See the published version at https://doi.org/10.1093/narcan/zcab022.

Abstract

Background: Chemotherapy intensifies pressure on the DNA repair pathways that can lead to deregulation. There is an urgent clinical need to be able to track the emergence of chemotherapy resistance and tailor patient staging appropriately. This is especially evident in the triple negative breast cancer (TNBC) subtype, of which standard of care is chemotherapy with tumours displaying high levels of inherent genome instability. TNBC has an overall poor prognosis for survival. There have been numerous studies into single agent chemoresistance but to date no study has elucidated in detail the roles of the key DNA repair components in resistance associated with the frontline clinical combination of anthracyclines and taxanes together.

Methods: In this study, we hypothesized that the emergence of chemotherapy resistance is driven by changes in functional signaling in the DNA repair pathways. We identified the importance of the DNA repair pathways in chemoresistant clinical samples and characterized the emergence of chemoresistance in TNBC cell lines. We utilized classical DNA repair assays and specific targeting of key DNA repair proteins to elucidate a new mechanism for adaptation to the combination of doxorubicin and docetaxel.

Results: We identified that consistent pressure on the non-homologous end joining pathway in the presence of genome instability causes failure of the key kinase DNA-PK, loss of p53 and compensation by p73. In-turn a switch to reliance on the homologous recombination pathway and RAD51 recombinase occurs to repair residual double strand DNA breaks.

Conclusions: We demonstrate that RAD51 is an actionable target for resensitization to chemotherapy in resistant cells with a matched gene expression profile of resistance highlighted by homologous recombination.

Background

The continued clinical use of chemotherapy for hard-to-treat cancers has meant that prospective emergence of chemotherapy resistance drives poor patient outcome (1). Invariably during relapse, the secondary cancers are resistant to the therapy initially utilized (2). For our studies, we exploited the triple negative breast cancer subtype to model chemotherapy resistance. Triple negative breast cancer (TNBC) is characterized by the absence of the therapeutically targetable hormone receptors namely estrogen, progesterone and human epidermal growth factor 2 expression receptors. TNBC is a fast-growing cancer that elicits pressure on the DNA repair pathways, even in the absence of therapy, via replication stress (3). Consequently, chemotherapy-induced DNA repair functions can become dysregulated resulting in hyper-repair or deficiency as a means to stabilize the cancer genome.

The major DNA double strand break repair pathways available to TNBC cells are the low fidelity, non-homologous-end joining pathway mediated by the kinase DNA-PK and the high fidelity homologous recombination repair pathway mediated by the recombinase RAD51 (4). The activation of the DNA damage response (DDR) is a result of cell cycle stage and availability of appropriate machinery in either

of the pathways. There are common genotypic trends in TNBC that guide the DDR, of note, virtually all (> 80%) TNBCs harbor p53 mutations (5, 6), 73% display RAD51 overexpression and 15% have BRCA1/2 mutations (7). In TNBC, overexpression of p53 promotes non-homologous end joining throughout the cell cycle by repressing RAD51 gene transcription and activating 53BP1 (8). In contrast, homologous recombination can be promoted in the $BRCA1^{mutant}$ subset via RAD51 overexpression compensation for BRCA1 loss (9). This is one of the molecular mechanisms observed for the low objective response rates of BRCA-mutant patients to PARP inhibitors (9). A variety of BRCA1-proficient tumour types also display high levels of nuclear RAD51 without DNA damage induction (10, 11), which suggests a role for RAD51 overexpression in tumorigenesis and possibly chemotherapy resistance (7, 9).

Currently measurement of DNA repair function is in clinical use as a diagnostic for TNBC. Homologous recombination deficiency (HRD) score is the arithmetic sum of chromosome instability based on somatic sequencing. These mutational signatures differ due to patient variation in aberrant DNA repair function (12). Clinically, HRD is an important metric in providing a “snapshot” for aberrant DNA repair, *BRCA*ness profile and chemoresistance (13). While HRD has found utility to identify patients likely to respond to PARP inhibitors there were no differences in objective response rates in patients with high or low HRD for chemotherapy that induces DNA damage, namely docetaxel and carboplatin in unselected patients (14). Furthermore, a functional assay for homologous recombination (RAD51 foci count) outperformed HRD in prognostic evaluation of patient response to PARP inhibition (15). Therefore, functional DDR mechanisms, expression and/or signaling may represent clinically relevant prognostic readouts beyond mutational scoring to guide therapeutic choices. We aim to take advantage of this dysregulation to elucidate and exploit key molecular drivers as complementary rational therapies for more accurate staging of TNBC.

Materials/methods

Cell culture

MDA-MB-231, MDA-MB-468, Hs578t and BT549 cells were sourced from the ATCC. Cells were confirmed to be negative for mycoplasma and authenticated by short tandem repeat analysis every 6 months. All lines were maintained in Dulbecco’s Modified Eagle Medium with 5% fetal bovine serum (FBS) and antibiotics, except BT549, which was maintained in RPMI with 5% FBS and antibiotics.

Chemotherapy adaption

Cell lines above were grown in the presence of ever-increasing doses of doxorubicin and docetaxel over the course of 6–8 months. Cellular death above 80% meant cells were allowed to recover for 1–2 weeks in media free of the chemotherapy combination.

Chemotherapy dose-response analysis, targeted treatment and readout

Cells were seeded in 24-well plates (5×10^4/well), then incubated for 72 h in the presence of docetaxel or doxorubicin (0-100μM), the combination of 1:100 docetaxel or doxorubicin referred to as “chemotherapy or CHEMO” (0.3 and 30 nM), small molecules targeting DNA-PK (0–1 mM),. Metabolic activity was assayed A 5 mg/mL stock solution was prepared with Thiazolyl Blue Tetrazolium Blue (MTT) and DPBS and read at 590 nm after 60 min incubation and dehydration with 10% total volume isopropanol.

Incucyte Zoom realtime growth analysis

Cell proliferation and/or cell death over time was evaluated by live cell imaging using the IncuCyte Zoom (Essen BioScience). For cell death assessment, Nuc Green Live dead reagent was added to culture medium (1:200) when treatment and vehicle control conditions were added. The Phase channel was used to measure cell proliferation/total cells (measured as % phase confluence) and the Green channel was used to detect cell death (measured as % green confluence). Plates were scanned at 3 hourly intervals to capture images. Data from IncuCyte Zoom was exported into Graphpad Prism to calculate the Area Under the Curve for Phase Confluence and Green Confluence.

Non-homologous end joining and Homologous recombination assay

In a 6-well plate, adherent cells were transiently transfected using Lipofectamine 2000 with 2 μg of linearized NHEJ reporter vector or pDR-GFP with 2 μg pCBAScel or 2 μg of circularized pEGFP-N1 (Clontech) to serve as a control for transfection efficiency in each assay. GFP expression was measured on the FACSCanto II flow cytometer (BD Biosciences) 72 hours later. Due to the differences in transfection efficiency between individual cell lines, linearized GFP was normalized back to circular GFP.

Immunofluorescence

In short, 5×10^4 cells were seeded onto 18 mm glass coverslips, then 24 h later, washed in PBS, fixed with cold 74% paraformaldehyde and permeabilized with 0.1% Triton X-100 for 15 min at room temperature (RT). Cells were blocked with 1% BSA, incubated with primary antibody (1:50 in 0.1% BSA + PBS, anti-Prion clone 3F4 Merck Cat# MAB1562) overnight at 4 °C then secondary antibody (1:500 Abcam, anti-mouse Cat#ab150113, anti-rabbit Cat#ab6564) for 30 min at RT. Immuno-stained cells were then washed, mounted with ProLong® Gold Antifade Mountant containing 4’,6’-diamidino-2-phenylindole (DAPI) for microscopy. Images were taken on a Zeiss 780-NLO confocal microscope.

Statistical analysis

Results are presented as mean +/- SEM of replicate analyses and are either representative or inclusive of at least three independent experiments. In all Figures, significant differences between specified pair of conditions were assessed using 2-tailed student’s *t*-tests, with *p* values *<0.01, **0 < 0.001, ***<0.0001, ****<0.00001 considered significant. Inhibitory concentration 50% (IC50) values were calculated by interpolation of sigmoidal dose-response curves produced from non-linear regression analyses.

Results

Chemoresistance to the combination of doxorubicin and docetaxel is efficiently achieved by loss of genetic material.

There is a clinical need to predict response following chemotherapy treatment and avoid unwarranted treatment and a cancer relapse. We analysed the clinical survival data for standard of care neoadjuvant taxane-anthracycline (docetaxel and doxorubicin) frontline combination therapy comparing TNBC with the remaining subtypes. Results showed that TNBC patients displayed significantly worse distant recurrence free survival (GSE25066, ****$p = 1.8^{e-6}$) (Fig. 1A). To evaluate the essential pathways observed in TNBC patients in response to neoadjuvant docetaxel and doxorubicin frontline combination, we analyzed the gene expression changes in treated patients, comparing TNBC to the Luminal/HER2 + subtypes (GSE25066)(16). Molecular Signatures Database curated gene set analysis resulted in differential induction of 88 genes, while 130 genes were repressed (Supplementary Table 1). The gene signatures were able to distinctly separate TNBC (Basal) from the remaining subtypes in GSE25066 (Fig S1A/B) and an independent dataset (Fig. 1B). Gene ontology molecular functions analysis of the TNBC-distinguishing gene signatures revealed four of the top 10 ranked, contained pathways with known DNA binding functions. Of these four, two included pathways with double strand DNA binding, which is functionally dominated by DNA repair proteins and associated functions (Fig. 1C). Although chemoresistance has been attributed to cancer stem-cells, no gene ontology annotated terms or molecular functions were assigned to stem-like functions or phenotypes. This may suggest a dominant role for DNA repair pathways in gene expression response to docetaxel and doxorubicin. In line with this, we observe a positive correlation between our above gene expression signatures (induced and repressed genes) and a gene expression signature, based on the expression of 230 genes as measure for homologous DNA repair deficiency (HRD) in basal breast cancer patients (Fig. 1D).

In order to evaluate the chemotherapy resistance mechanisms driving TNBC recurrence, we grew four TNBC cell lines MDA-MB-231, Bt549, Hs578t and MDA-MB-468 and exposed them to the frontline therapy combination of doxorubicin and docetaxel (ratio 100:1) starting at 0.1 nM docetaxel and 10 nM doxorubicin and concluding with 2 nM docetaxel and 200 nM doxorubicin. The concentration was chosen to mimic the clinical administration of bolus doxorubicin and infusion of docetaxel (17). Resistance was achieved over 6–8 months with escalating doses of the chemotherapy combination. Chemotherapy resistance has been shown to correlate with acquisition of new genomic aberrations and adaptive copy-number evolution (18). To investigate this, we performed metaphase spread counts comparing chromosome numbers between sensitive and resistant paired lines. On a macromolecular level all resistant cell lines had an overall loss of genetic material compared to sensitive parental cells. There was significant loss in chromosome count in the MDA-MB-231 (Fig. 1E) and BT549 (Fig. 1F) and trended lower in Hs578t (Fig. 1G) and MDA-MB-468 cells (Fig. 1H) but did not reach statistical significance. The two statistically significant lines correlated with higher IC50 values achieved for docetaxel (Fig. 1I) and there was a strong correlation between chromosome loss and resistance to docetaxel (Fig. 1J). This observation was repeated with doxorubicin (Fig. 1K/L). This suggests that adaptation to DNA damaging

agents requires or results in loss of genetic material. A more detailed analysis of copy number variation in resistant MDA-MB-231 and MDA-MB-468 lines confirmed the observations made with our metaphase spread data (Fig S2). The more highly resistant MDA-MB-231 genetics displayed a greater increase in loss of heterozygosity and a reduction in copy number gains compared to the MDA-MB-468 resistant line (Fig S2). In addition, there was a positive correlation between the TNBC-distinguishing gene signatures and several measures of genomic instability, including the CIN70 gene expression signature (functional aneuploidy), overall aneuploidy and chromosome arm aneuploidy burden (Fig S3). Overall, we observed a correlation between chemotherapy-induced gene expression specifically in TNBC and DDR pathway activation/genome instability. We also observed a correlation between genome instability and levels of resistance achieved.

Chemoresistance drives a shift towards homologous recombination to sustain genome stability.

To evaluate the role of the individual DNA repair pathways in the observed chemoresistance profiles, we analysed the specific cellular double strand DNA break repair response. The two main double strand break DNA repair pathways are the error prone non-homologous end-joining pathway and high-fidelity homologous recombination pathway. We utilized the classical enzyme directed double strand DNA break of GFP and the MDA-MB-231 matched pair sensitive and resistant lines. The first assay was a measure of homologous recombination activity and required a sister template of GFP (iGFP) and active pathway to recapitulate the fluorescence of an enzyme cleaved GFP construct (Fig. 2A). In contrast to our expectations, related to genetic losses via high levels of error prone non-homologous end joining repair, the MDA-MB-231RES cells displayed significantly enhanced homologous recombination activity with 7-fold higher activity compared to MDA-MB-231^{SENS} (**$p < 0.001$, Fig. 2B). The second assay was a measure of non-homologous end joining via recapitulation of the upstream gene cassette with active promoter for GFP expression (Fig. 2C). Although to a much lesser extent, MDA-MB-231RES cells also displayed enhanced non-homologous end-joining 2.8-fold (***$p < 0.001$, Fig. 2D). Thus, acquired chemotherapy resistant cells rely upon enhanced DNA repair in both of the main double strand break repair pathways.

To determine whether the adapted cells are reliant upon any specific pathway, we inhibited repair with specific small molecule inhibitors in the context of cell death via DNA double strand breaks induced by gamma irradiation (Fig. 2E). A cellular response to ATM inhibition would represent a general activation of double strand break response, while a response to ATR inhibition would represent a reliance upon single strand break response repair. Specific targeting of key repair proteins provides further insights. Cell death in response to DNA-PK inhibition represents a reliance upon non-homologous end joining, while cell death induced by RAD51 inhibition shows cellular reliance upon homologous recombination. Finally, PARP inhibition is a measure of reliance upon alternative non-homologous end joining. Comparing cell death induced by each of the inhibitors, we observed a switch from an equal distribution between the available repair mechanisms of alternative-non homologous end joining, non-homologous end joining and homologous recombination pathways in MDA-MB-231^{SENS} to a dominant homologous recombination

dependent phenotype in MDA-MB-231RES (Fig. 2E, bottom panel). The same shift towards homologous recombination was observed when DNA double strand breaks were induced by the combination of docetaxel and doxorubicin in MDA-MB-231 lines (Fig. 2F). The BT549 cell line, like MDA-MB-231, also displayed significant difference in chromosome count and, consistent with this, displayed the same shift towards reliance on the homologous recombination pathway when resistant to the combination of docetaxel and doxorubicin (Fig. 2G).

To evaluate whether the increased reliance on homologous recombination was related to higher levels of DNA damage, RAD51 function or even longer time spent in S-G2 phase where homologous recombination is active, we analyzed the resolution of DNA double strands breaks over a 24-hour time course in BT549 and MDA-MB-231 cells, respectively (Fig. 2H and S4). Double strand breaks are visualized within the nucleus by gamma-H2AX foci marks. Active double strand break repair is visualized and attributed to homologous recombination as RAD51 foci, while the switch to activate non-homologous end joining is visualized with 53BP1 foci. Compared to BT549^{SENS} cells, (Fig. 2H) BT549^{RES} cells (Fig. 2I) had a higher RAD51 foci count per nucleus, although these formed with slower kinetics than in the sensitive cells. Although the cells display slower RAD51 kinetics, BT549^{RES} cells resulted in enhanced resolution of gamma-H2Ax foci (DNA double strand breaks) at the 24-hour time point, as compared to the BT549^{SENS} cells treated with the same dose of IR (Fig. 2H vs 2I). BT549^{RES} and BT549^{SENS} displayed similarly low levels of 53BP1 induction following IR treatment, consistent with similar signaling towards non-homologous end joining (Fig. 2H vs 2I). This data supports our inhibitor results and showed that resistant cells utilize homologous recombination, sustain the same amplitude of double strand breaks as sensitive cells but resolve these breaks more efficiently.

Sensitization of chemoresistant cells by targeting RAD51 and homologous recombination.

Having established an enhanced homologous recombination repair phenotype in chemoresistant cell lines, we wondered if targeting of the key repair protein RAD51 could sensitize these cells. Utilizing a validated small molecule inhibitor of RAD51 (19), MDA-MB-231RES were actually significantly more sensitive to the inhibitor than MDA-MB-231SENS cells (Fig. 3A). The combination of chemotherapy and RAD51 inhibition achieved resensitization and equivalent levels of cell death independent of chemoresistance status (Fig. 3A). Conversely, stabilization of RAD51 with a small molecule (RS-1)(20) congruently enhanced chemotherapy resistance in MDA-MB-231RES (Fig. 3B). Therefore, RAD51 function demonstrated a direct role of homologous recombination in chemoresistance.

The targeting of RAD51 with chemotherapy induced cell death irrespective of chemoresistance. This provides the capability to successfully target the heterogeneity often observed in TNBC. However, we find that the functionally available repair pathways in sensitive and resistant lines are very different. We evaluated the gene expression profile as a readout for DNA damage response to the combination of chemotherapy and RAD51i (Fig. 3A). Utilizing a targeted array of 21 DNA repair related genes and cluster analysis per individual gene in MDA-MB-231^{SENS} cells we revealed 15/21 of the genes were most highly induced by chemotherapy and RAD51i (Fig. 3C). The Euclidean distance arranged these genes into three

main clusters, each of which were derived of both key non-homologous end joining and homologous recombination pathways, cluster I-BRCA1 and DNA-PK, cluster II-KU70 and BRCA2 and cluster III PARP1 and KU80. This was representative of an even distribution of DDR pathways utilized and similar to what was observed in our small molecule inhibition studies in MDA-MB-231^{SENS} cells (Fig. 2F). The induction of gene expression is a representation of individual gene response however we were curious about the functional response. Therefore, we performed functional interaction network analysis and displayed distances based on physical, colocalization and co-expression values. The most highly expressed genes circled in red were tightly associated by physical interactions (pink lines) and outliers joined by pathway association (blue lines) (Fig. 3D).

Analysis of MDA-MB-231RES cells, revealed only 5/21 of the genes were most highly induced by chemotherapy and RAD51i (Fig. 3E). These genes were functionally associated with inhibition of non-homologous end joining, cluster I-p73, cluster II-PARP1, cluster III-cABL1 and no highly expressed genes in cluster IV (Fig. 3E). Functional interaction network analysis revealed that RAD51 was again centrally located in the network and closely associated with cABL1 and BRCA1 (Fig. 3F). Notably RAD51 was also induced in response to chemotherapy alone in both cell lines and as it is centrally located in each network it is a rationale target in TNBC tumours that often display chemoresistance heterogeneity.

Gene ontology molecular functions analysis of the 21 genes revealed that the MDA-MB-231^{SENS} continued to rely upon both homologous recombination and non-homologus end joining as two of the top 10 pathways while MDA-MB-231RES relied upon only homologous recombination (Figs. 3G/H). Supporting protein analysis of MDA-MB-231RES revealed that DNA-PK did not display the classical phosphorylation in response to chemotherapy as seen in MDA-MB-231^{SENS}, although total DNA-PK protein expression was sustained (Fig. 3I). This suggested non-functional or ablated non-homologous end joining activity. We also observed associated increases in 53BP1 protein expression in MDA-MB-231RES across all treatment conditions supporting activation of DNA-PK and non-homologous end joining activity (Fig. 3I). RAD51 protein expression was not enhanced and there was an associated loss of BRCA1 expression, suggesting suppression of homologous recombination. However, we also observed a compensation by enhanced BRCA2 expression in MDA-MB-231RES cells. In addition, we observed an induction of p73 with associated repression of p53 activation, providing a switch in DNA damage sensing to p73.

Discussion

A better understanding of the early events of the adaptive response to chemotherapy are urgently needed for the timely detection of chemoresistance and therapeutic interventions against tumour relapse. Our previous work supports the hypothesis that high RAD51 expression and homologous recombination reliance is a late stage event supporting patient relapse and metastasis (7). Our current findings show early reliance upon non-homologous end joining and DNA-PK activity under genome instability conditions resulted in a loss of genetic material. In support of genomic instability and DDR driving early drug

adaption, Hansen *et al* identified major genomic variations midway through docetaxel adaption (21) and Tsou *et al*, the attenuation of DNA repair proteins BRCA1/2 and wild type p53 early in adaption to doxorubicin (22).

We suspected from hierarchical clustering that loss of mutant p53 and DNA-PK dysfunction are early events followed by reduced 53BP1 expression in selected clonal expansion rather than general pathway regulation (Fig. 4). TNBC patient tumours and derived cell lines each harbour high levels of replication stress. Replication stress, is defined by a dependence upon ATR activation due to extended single stranded DNA at the replication fork (23). Therefore baseline levels of aberrant DNA repair is already high and associated chromosome instability can be tolerated promoting diversification of subclones (24). Our TNBC sensitive cell lines displayed instability with baseline ATR dependence and therefore were primed for genetic loss. A recent melanoma study, Kwong *et al* showed under strong selective pressure, genetically stable tumours (diploid) acquired resistance via mutation and activation of oncogenic pathways, whereas genomically unstable tumours acquired resistance via broad whole chromosome aneuploidy (25). This mechanism was also reflected in TNBC patients with poor response to chemotherapy associated with higher levels of aneuploidy prior to treatment (26). This suggests clonal diversity is derived from pressure on the DDR and aberrant DNA repair preceding multidrug resistance phenotypes.

Almost all TNBC harbor TP53 mutations, with 82% of patients displaying somatic alterations (6). Most TP53 mutations confer resistance to drugs that directly target DNA or DNA synthesis (27). In our study, the lines that achieved the highest levels of resistance, MDA-MB-231 and BT549, have R280K and R249S p53 gain-of-function missense mutations, respectively. These mutations reduce DNA binding and infers reduced activation of cell death pathways (28, 29). Cancer cells that harbor mutation of p53 modulate induction of apoptosis through p73 (30). p73 is most commonly thought to act as a tumour suppressor via induction of cell death pathways under oncogenic stress. We observed a loss of function in mutant p53 after drug adaptation, however with no associated induction of apoptosis via p73 (31). This is likely due to the exclusive expression of the ΔNp73 isoform that acts as a dominant-negative inhibitor. ΔNp73 competes with p53, TAp63 and TAp73 for promoter binding and inhibits the activation of target genes, thereby blocking apoptosis (32). Indeed, we did not see induction of the classical apoptosis target gene PUMA in any of the cell lines we tested. In addition to evading apoptosis, we suggest that ΔNp73 contributed to the switch to dependence on homologous recombination. In contrast to TAp73, ΔNp73 binds 53BP1 inhibiting function, therefore depleting 53BP1 foci recruitment at DSBs and repressing non-homologous end joining (33). Therefore, in contrast to serving as a tumour suppressor, we and others suggest that ΔNp73 acts as an oncogene (34) notably during emergence of chemoresistance and DNA damage response crisis switch.

Targeting the DDR to resensitize chemoresistant cancers is yet to be fully realized. One of the few clinical examples demonstrated a significant increase in objective response activity in platinum-resistant ovarian cancer patients when a WEE1 inhibitor was added (35). The targeting of DNA-PK has yet to be tested in breast cancer. Some efficacy has been shown against haematological malignancies and activity in vitro

against MDA-MB-231, however we would be concerned about promoting the resistant profile we defined. We suggest the downstream homologous recombination effector, RAD51, as a rational clinical target to re-sensitize to chemotherapy in a contextual synthetic lethality response (36). Several strategies for targeting RAD51 are under development including small molecule inhibitors and antibody fragments (37, 38). Currently an oral RAD51 inhibitor CYT-0851 is being tested in a Phase 1/2 study against relapsed/refractory B-cell malignancies and advanced solid tumours including breast cancer (NCT03997968). We eagerly await the results and suggest its use for refractory TNBC.

Conclusion

High relapse rates, metastatic dissemination and poor prognosis for chemotherapy treated TNBC are all driven by the cellular response to DNA damage in the context of genome instability. We identified a potential gene expression profile to help predict when standard chemotherapy is failing and validated the use of DNA repair targeting agent in in a contextual synthetic lethality response. We hope to validate our findings in the future with relapse patient breast cancer organoids.

Abbreviations

Triple negative breast cancer (TNBC)

DNA damage response (DDR)

Homologous recombination deficiency (HRD)

fetal bovine serum (FBS)

room temperature (RT)

Inhibitory concentration 50% (IC50)

Declarations

Ethics approval and consent to participate: Not Applicable

Consent for publication: All authors have read the manuscript and agree to submission.

Availability of data and materials: All authors agree to open access to data and materials. The datasets generated for Fig 1A-D are available in the NCBI GEO “Genomic predictor of response and survival following neoadjuvant taxane-anthracycline chemotherapy in breast cancer, https://www.ncbi.nlm.nih.gov/geo/query/acc.cgi?acc=gse25066 .

Competing interests: There are no competing interests to declare.

Funding: This study was supported by funding Breast Friends Philanthropic fundraising.

Authors' contributions: APW JSL, DJR designed experiments, coordinated collaborations, and performed data analyses. AW and RVO created and validated drug adapted cell lines, executed most of the experiments and performed data analyses. PHGD and MCS analyzed clinical gene expression profiling and pathway analysis. GK validated gene expression in cell lines. SWM provided critical review and experimental design.

Acknowledgements: We would like to thank A/Prof. Fares Al-Ejeh, Qatar Biomedical Research Institute for critical review and feedback on this manuscript.

References

1. Nedeljković M, Damjanović A. Mechanisms of Chemotherapy Resistance in Triple-Negative Breast Cancer—How We Can Rise to the Challenge. Cells. 2019. doi:10.3390/cells8090957.
2. Masoodi T, Siraj S, Siraj AK, Azam S, Qadri Z, Parvathareddy SK, et al. Genetic heterogeneity and evolutionary history of high-grade ovarian carcinoma and matched distant metastases. Br J Cancer. 2020. doi:10.1038/s41416-020-0763-4.
3. Zhang J, Dai Q, Park D, Deng X. Targeting DNA replication stress for cancer therapy. Genes. 2016. doi:10.3390/genes7080051.
4. Helleday T, Petermann E, Lundin C, Hodgson B, Sharma RA. DNA repair pathways as targets for cancer therapy. Nat Rev Cancer. 2008. doi:10.1038/nrc2342.
5. Jin MS, Park IA, Kim JY, Chung YR, Im SA, Lee KH, et al. New insight on the biological role of p53 protein as a tumor suppressor: re-evaluation of its clinical significance in triple-negative breast cancer. Tumor Biol. 2016. doi:10.1007/s13277-016-4990-5.
6. Pareja F, Geyer FC, Marchiò C, Burke KA, Weigelt B, Reis-Filho JS. Triple-negative breast cancer: The importance of molecular and histologic subtyping, and recognition of low-grade variants. npj Breast Cancer. 2016. doi:10.1038/npjbcancer.2016.36.
7. Wiegmans AP, Al-Ejeh F, Chee N, Yap P-Y, Gorski JJ, Da Silva L, et al. Rad51 supports triple negative breast cancer metastasis. Oncotarget. 2014;5(10). doi:10.18632/oncotarget.1923.
8. Arias-Lopez C, Lazaro-Trueba I, Kerr P, Lord CJ, Dexter T, Iravani M, et al. p53 modulates homologous recombination by transcriptional regulation of the RAD51 gene. EMBO Rep. 2006. doi:10.1038/sj.embor.7400587.
9. Martin RW, Orelli BJ, Yamazoe M, Minn AJ, Takeda S, Bishop DK. RAD51 up-regulation bypasses BRCA1 function and is a common feature of BRCA1-deficient breast tumors. Cancer Res. 2007. doi:10.1158/0008-5472.CAN-07-0290.
10. Mitra A, Jameson C, Barbachano Y, Sanchez L, Kote-Jarai Z, Peock S, et al. Overexpression of RAD51 occurs in aggressive prostatic cancer. Histopathology. 2009. doi:10.1111/j.1365-2559.2009.03448.x.
11. Raderschall E, Stout K, Freier S, Suckow V, Schweiger S, Haaf T. Elevated levels of Rad51 recombination protein in tumor cells. Cancer Res. 2002.

12. Helleday T, Eshtad S, Nik-Zainal S. Mechanisms underlying mutational signatures in human cancers. Nat Rev Genet. 2014. doi:10.1038/nrg3729.
13. Telli ML, Hellyer J, Audeh W, Jensen KC, Bose S, Timms KM, et al. Homologous recombination deficiency (HRD) status predicts response to standard neoadjuvant chemotherapy in patients with triple-negative or BRCA1/2 mutation-associated breast cancer. Breast Cancer Res Treat. 2018. doi:10.1007/s10549-017-4624-7.
14. Tutt A, Tovey H, Cheang MCU, Kernaghan S, Kilburn L, Gazinska P, et al. Carboplatin in BRCA1/2-mutated and triple-negative breast cancer BRCAness subgroups: The TNT Trial. Nat Med. 2018. doi:10.1038/s41591-018-0009-7.
15. Castroviejo-Bermejo M, Cruz C, Llop-Guevara A, Gutiérrez-Enríquez S, Ducy M, Ibrahim YH, et al. A RAD 51 assay feasible in routine tumor samples calls PARP inhibitor response beyond BRCA mutation. EMBO Mol Med. 2018. doi:10.15252/emmm.201809172.
16. Hatzis C, Pusztai L, Valero V, Booser DJ, Esserman L, Lluch A, et al. A genomic predictor of response and survival following taxane-anthracycline chemotherapy for invasive breast cancer. JAMA - J Am Med Assoc. 2011. doi:10.1001/jama.2011.593.
17. Rajappa S, Joshi A, Doval DC, Batra U, Rajendranath R, Deo A, et al. Novel formulations of docetaxel, paclitaxel and doxorubicin in the management of metastatic breast cancer. Oncol Lett. 2018. doi:10.3892/ol.2018.9057.
18. Kim C, Gao R, Sei E, Brandt R, Hartman J, Hatschek T, et al. Chemoresistance Evolution in Triple-Negative Breast Cancer Delineated by Single-Cell Sequencing. Cell. 2018. doi:10.1016/j.cell.2018.03.041.
19. Ward A, Dong L, Harris JM, Khanna KK, Al-Ejeh F, Fairlie DP, et al. Quinazolinone derivatives as inhibitors of homologous recombinase RAD51. Bioorganic Med Chem Lett. 2017;27(14). doi:10.1016/j.bmcl.2017.05.039.
20. Jayathilaka K, Sheridan SD, Bold TD, Bochenska K, Logan HL, Weichselbaum RR, et al. A chemical compound that stimulates the human homologous recombination protein RAD51. Proc Natl Acad Sci U S A. 2008. doi:10.1073/pnas.0808046105.
21. Hansen SN, Ehlers NS, Zhu S, Thomsen MBH, Nielsen RL, Liu D, et al. The stepwise evolution of the exome during acquisition of docetaxel resistance in breast cancer cells. BMC Genom. 2016. doi:10.1186/s12864-016-2749-4.
22. Tsou SH, Chen TM, Hsiao HT, Chen YH. A critical dose of doxorubicin is required to alter the gene expression profiles in MCF-7 cells acquiring multidrug resistance. PLoS One. 2015. doi:10.1371/journal.pone.0116747.
23. Cimprich KA, Cortez D. ATR: An essential regulator of genome integrity. Nat Rev Mol Cell Biol. 2008. doi:10.1038/nrm2450.
24. Rowald K, Mantovan M, Passos J, Buccitelli C, Mardin BR, Korbel JO, et al. Negative Selection and Chromosome Instability Induced by Mad2 Overexpression Delay Breast Cancer but Facilitate Oncogene-Independent Outgrowth. Cell Rep. 2016. doi:10.1016/j.celrep.2016.05.048.

25. Kwong LN, Zou L, Chagani S, Pedamallu CS, Liu M, Jiang S, et al. Modeling Genomic Instability and Selection Pressure in a Mouse Model of Melanoma. Cell Rep. 2017. doi:10.1016/j.celrep.2017.04.065.
26. Kim H, Zheng S, Amini SS, Virk SM, Mikkelsen T, Brat DJ, et al. Whole-genome and multisector exome sequencing of primary and post-treatment glioblastoma reveals patterns of tumor evolution. Genome Res. 2015. doi:10.1101/gr.180612.114.
27. Liu C, Banister CE, Buckhaults PJ. Spindle assembly checkpoint inhibition can resensitize p53-null stem cells to cancer chemotherapy. Cancer Res. 2019. doi:10.1158/0008-5472.CAN-18-3024.
28. Leroy B, Girard L, Hollestelle A, Minna JD, Gazdar AF, Soussi T. Analysis of TP53 mutation status in human cancer cell lines: A reassessment. Hum Mutat. 2014. doi:10.1002/humu.22556.
29. Gomes AS, Trovão F, Andrade Pinheiro B, Freire F, Gomes S, Oliveira C, et al. The crystal structure of the R280K mutant of human p53 explains the loss of DNA binding. Int J Mol Sci. 2018. doi:10.3390/ijms19041184.
30. Bergamaschi D, Gasco M, Hiller L, Sullivan A, Syed N, Trigiante G, et al. p53 polymorphism influences response in cancer chemotherapy via modulation of p73-dependent apoptosis. Cancer Cell. 2003. doi:10.1016/S1535-6108(03)00079-5.
31. Bae YH, Ryu JH, Park HJ, Kim KR, Wee HJ, Lee OH, et al. Mutant p53-Notch1 signaling axis is involved in curcumin-induced apoptosis of breast cancer cells. Korean J Physiol Pharmacol. 2013. doi:10.4196/kjpp.2013.17.4.291.
32. Oswald C, Stiewe T. In good times and bad: p73 in cancer. Cell Cycle. 2008. doi:10.4161/cc.7.12.6148.
33. Di C, Yang L, Zhang H, Ma X, Zhang X, Sun C, et al. Mechanisms, function and clinical applications of DNp73. Cell Cycle. 2013. doi:10.4161/cc.24967.
34. Stiewe T, Zimmermann S, Frilling A, Esche H, Pützer BM. Transactivation-deficient δTA-p73 acts as an oncogene. Cancer Res. 2002.
35. Leijen S, Van Geel RMJM, Sonke GS, De Jong D, Rosenberg EH, Marchetti S, et al. Phase II study of WEE1 inhibitor AZD1775 plus carboplatin in patientswith tp53-mutated ovarian cancer refractory or resistant to first-line therapy within 3 months. J Clin Oncol. 2016. doi:10.1200/JCO.2016.67.5942.
36. O'Connor MJ. Targeting the DNA Damage Response in Cancer. Mol Cell. 2015. doi:10.1016/j.molcel.2015.10.040.
37. Ward A, Khanna KK, Wiegmans AP. Targeting homologous recombination, new pre-clinical and clinical therapeutic combinations inhibiting RAD51. Cancer Treat Rev. 2015;41(1). doi:10.1016/j.ctrv.2014.10.006.
38. Pastushok L, Fu Y, Lin L, Luo Y, DeCoteau JF, Lee K, et al. A Novel Cell-Penetrating Antibody Fragment Inhibits the DNA Repair Protein RAD51. Sci Rep. 2019. doi:10.1038/s41598-019-47600-y.
39. Peng G, Lin CCJ, Mo W, Dai H, Park YY, Kim SM, et al. Genome-wide transcriptome profiling of homologous recombination DNA repair. Nat Commun. 2014. doi:10.1038/ncomms4361.

Figures

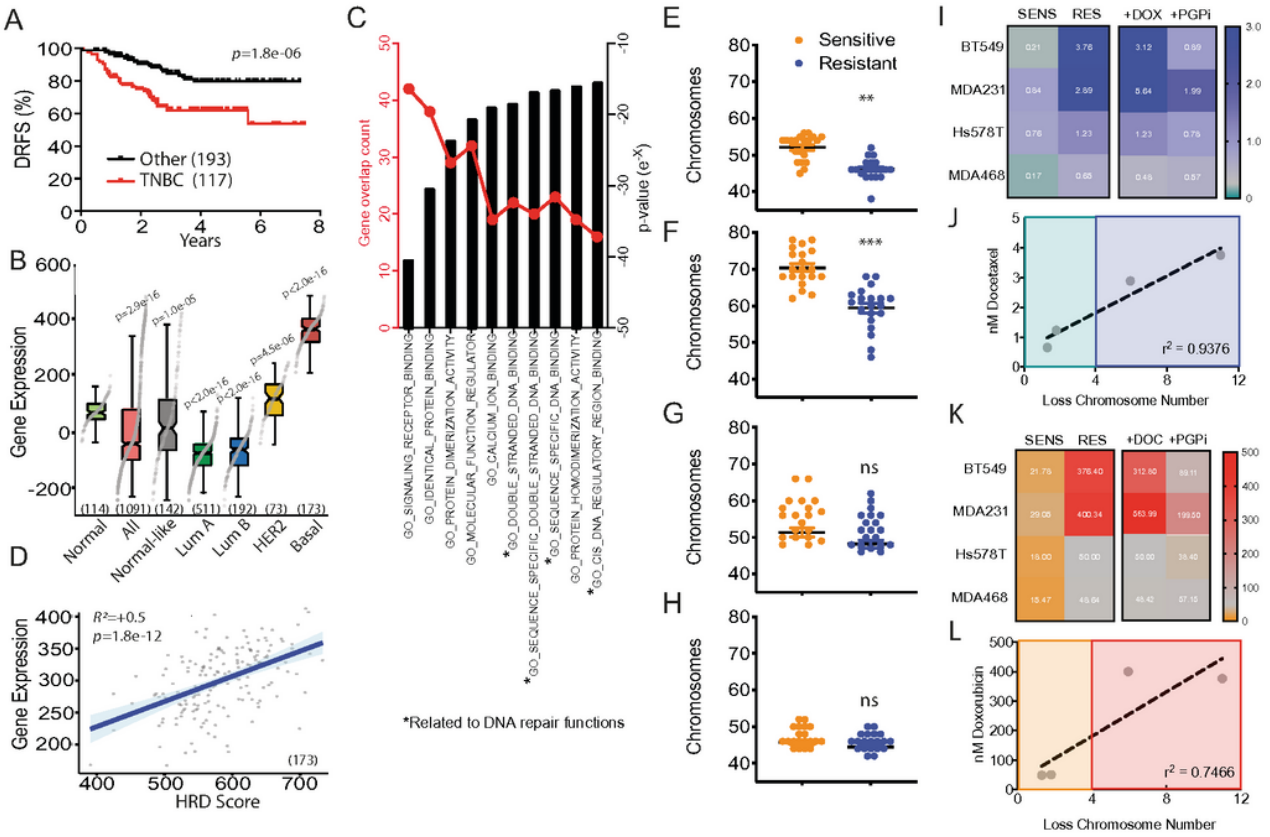

Figure 1

Evaluation of TNBC genome stability traits from clinical trials and drug adapted cell lines. A Distance relapse free survival of neoadjuvant doxorubicin and docetaxel treated patients stratified for triple negative breast cancer subtype versus the remaining subtypes (GSE25066; 310 patients in total). p=1.8e-6 Log-rank Mantel-Cox test. B Genes induced in response to chemotherapy combination doxorubicin and docetaxel profile expressed in each of the breast cancer subtypes (GSE25066). Mann-Whitney U test p-values as shown. C Molecular signatures Database curated gene set comparing TNBC to other subtypes for gene expression changes in molecular functions ranked based on gene numbers and statistical significance following neoadjuvant doxorubicin and docetaxel chemotherapy (GSE25066). D Patient samples compared for genes expression induced in response to chemotherapy combination doxorubicin and docetaxel profile compared to Homologous recombination deficiency measured using a gene expression signature, based on the expression of 230 genes (HRD_score), as previously reported (39). E Chromosome count of metaphase spreads comparing MDA-M-231 sensitive and resistant cell lines. F BT549, G Hs578t and H MDA-MB-468(***p<0.0001, **p<0.001 paired student t-test, +/- SEM of 3 independent experiments). I Heat map of IC50 values derived from dose curves for each matched sensitive (SENS) and drug adapted (RES) TNBC cell lines for docetaxel monotherapy, in combination with

doxorubicin and with the addition of p-glycoprotein pump inhibitor (PGPi). IC50 (nM) indicated from 3 independent experiments. J Correlation between IC50 of docetaxel and the average loss of chromosome number observed in the matched resistant cell line. r2=0.9376 Pearson correlation coefficient, *p=0.034 paired student t-test. K As above in I, heat map utilizing doxorubicin monotherapy in combination with docetaxel and with the addition of p-glycoprotein pump inhibitor (PGPi). L Correlation between IC50 of doxorubicin and the average loss of chromosome number observed in the matched resistant cell line. r2=0.7466 Pearson correlation coefficient, ns.

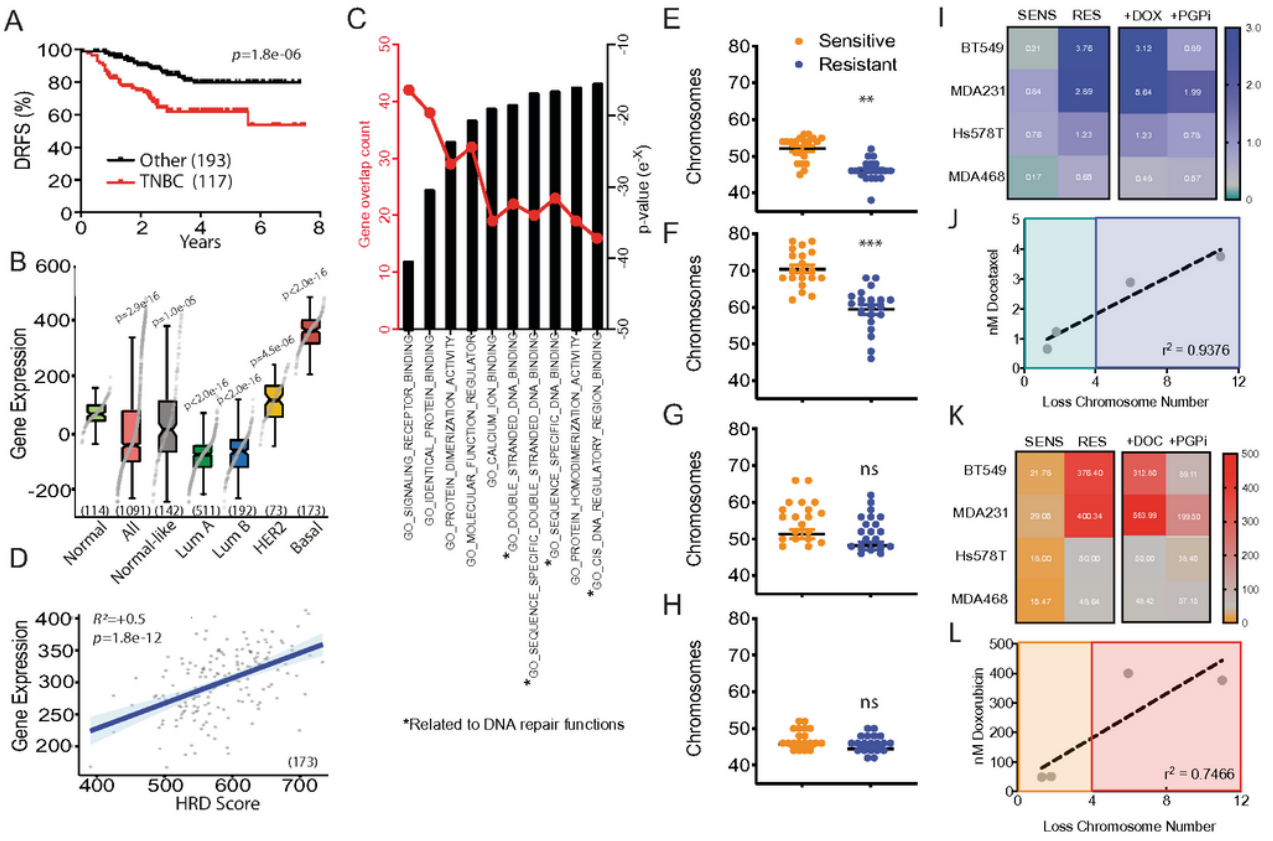

Figure 1

Evaluation of TNBC genome stability traits from clinical trials and drug adapted cell lines. A Distance relapse free survival of neoadjuvant doxorubicin and docetaxel treated patients stratified for triple negative breast cancer subtype versus the remaining subtypes (GSE25066; 310 patients in total). p=1.8e-6 Log-rank Mantel-Cox test. B Genes induced in response to chemotherapy combination doxorubicin and docetaxel profile expressed in each of the breast cancer subtypes (GSE25066). Mann-Whitney U test p-values as shown. C Molecular signatures Database curated gene set comparing TNBC to other subtypes for gene expression changes in molecular functions ranked based on gene numbers and statistical significance following neoadjuvant doxorubicin and docetaxel chemotherapy (GSE25066). D Patient samples compared for genes expression induced in response to chemotherapy combination doxorubicin and docetaxel profile compared to Homologous recombination deficiency measured using a gene

expression signature, based on the expression of 230 genes (HRD_score), as previously reported (39). E Chromosome count of metaphase spreads comparing MDA-M-231 sensitive and resistant cell lines. F BT549, G Hs578t and H MDA-MB-468(***p<0.0001, **p<0.001 paired student t-test, +/- SEM of 3 independent experiments). I Heat map of IC50 values derived from dose curves for each matched sensitive (SENS) and drug adapted (RES) TNBC cell lines for docetaxel monotherapy, in combination with doxorubicin and with the addition of p-glycoprotein pump inhibitor (PGPi). IC50 (nM) indicated from 3 independent experiments. J Correlation between IC50 of docetaxel and the average loss of chromosome number observed in the matched resistant cell line. r2=0.9376 Pearson correlation coefficient, *p=0.034 paired student t-test. K As above in I, heat map utilizing doxorubicin monotherapy in combination with docetaxel and with the addition of p-glycoprotein pump inhibitor (PGPi). L Correlation between IC50 of doxorubicin and the average loss of chromosome number observed in the matched resistant cell line. r2=0.7466 Pearson correlation coefficient, ns.

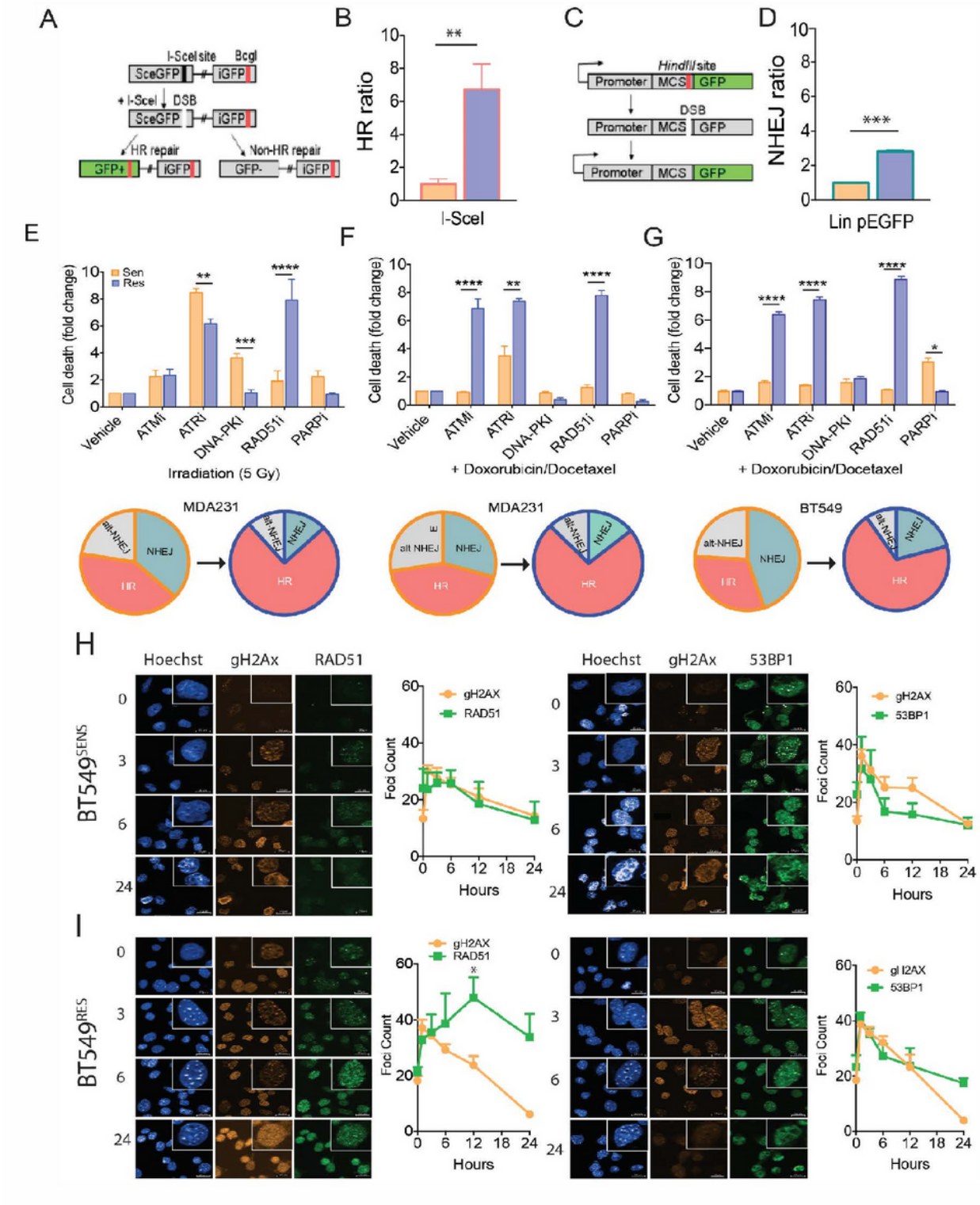

Figure 2

Functional shift in DNA damage response in drug adapted cell lines. A Schematic diagram of DNA repair GFP fluorescent reporter for homologous recombination driven repair of I-Sce1 enzyme-mediated double strand break. B Sensitive and resistant MDA-MB-231 were assayed for homologous recombination activity in non-synchronized cells. **p<0.001 paired student t-test, +/- SEM of 3 independent experiments. C Schematic diagram of DNA repair GFP fluorescent reporter for Non-homologous end joining driven

repair of linearized GFP. D Sensitive and resistant MDA-MB-231 were assayed for non-homologous end joining activity in non-synchronized cells (***p<0.0001 Paired student t-test, +/- SEM of 3 independent experiments). E MDA-MB-231 cells monitored for cell growth over 5 days with incucyte live cell imaging and dead cells selected for with a cell-impermeant dye. Response was compared for irradiation induced double strand breaks inhibition of key proteins against homologous recombination (RAD51), non-homologous end joining (DNA-PK), alternative non-homologous end joining (PARP) and key upstream signaling kinases (ATM and ATR)(***p<0.0001 Paired student t-test, +/- SEM of 3 independent experiments). Change in repair pathway dependence is also expressed as a proportion of total cell death. F Matched sensitive and resistant MDA-MB-231 cells lines were assayed as above, however double strand breaks were induced by the combined activity of doxorubicin and docetaxel (****p<0.00001, **p<0.001 paired student t-test, +/- SEM of 3 independent experiments). G Matched sensitive and resistant BT549 cells lines were assayed as above, however double strand breaks were induced by the combined activity of doxorubicin and docetaxel (****p<0.00001, **p<0.001 paired student t-test, +/- SEM of 3 independent experiments). H Immunofluorescent analysis of the rate of double strand break repair marked by comparison of gammaH2AX foci marked breaks, homologous recombination RAD51 foci and 53BP1 foci as a marker for switch to non-homologous end joining in BT549 sensitive cells. I Immunofluorescent analysis of the rate of double strand break repair marked by comparison of gammaH2AX foci marked breaks, homologous recombination RAD51 foci and 53BP1 foci as a marker for switch to non-homologous end joining in BT549 resistant cells.

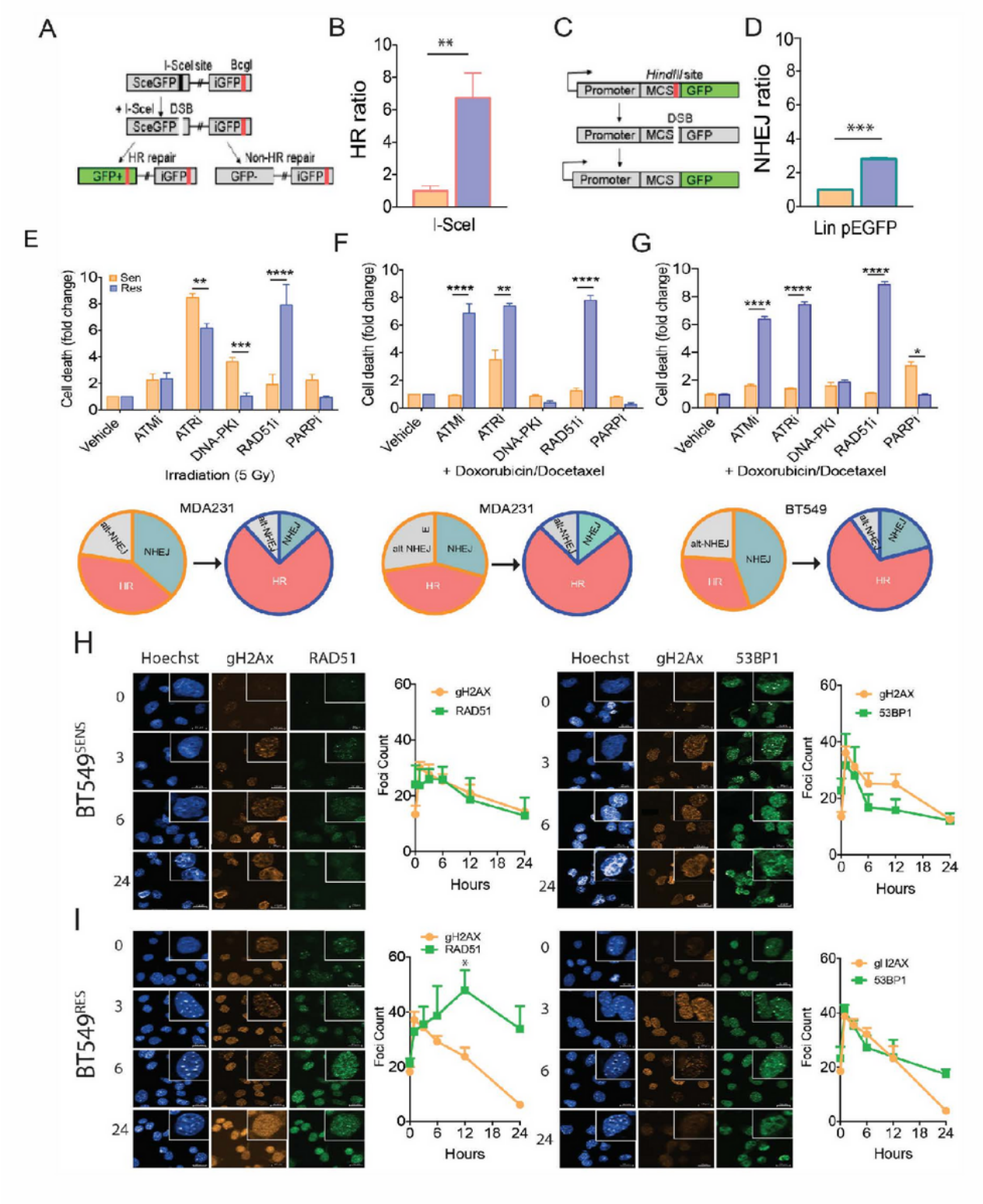

Figure 2

Functional shift in DNA damage response in drug adapted cell lines. A Schematic diagram of DNA repair GFP fluorescent reporter for homologous recombination driven repair of I-Sce1 enzyme-mediated double strand break. B Sensitive and resistant MDA-MB-231 were assayed for homologous recombination activity in non-synchronized cells. **p<0.001 paired student t-test, +/- SEM of 3 independent experiments. C Schematic diagram of DNA repair GFP fluorescent reporter for Non-homologous end joining driven

repair of linearized GFP. D Sensitive and resistant MDA-MB-231 were assayed for non-homologous end joining activity in non-synchronized cells (***p<0.0001 Paired student t-test, +/- SEM of 3 independent experiments). E MDA-MB-231 cells monitored for cell growth over 5 days with incucyte live cell imaging and dead cells selected for with a cell-impermeant dye. Response was compared for irradiation induced double strand breaks inhibition of key proteins against homologous recombination (RAD51), non-homologous end joining (DNA-PK), alternative non-homologous end joining (PARP) and key upstream signaling kinases (ATM and ATR)(***p<0.0001 Paired student t-test, +/- SEM of 3 independent experiments). Change in repair pathway dependence is also expressed as a proportion of total cell death. F Matched sensitive and resistant MDA-MB-231 cells lines were assayed as above, however double strand breaks were induced by the combined activity of doxorubicin and docetaxel (****p<0.00001, **p<0.001 paired student t-test, +/- SEM of 3 independent experiments). G Matched sensitive and resistant BT549 cells lines were assayed as above, however double strand breaks were induced by the combined activity of doxorubicin and docetaxel (****p<0.00001, **p<0.001 paired student t-test, +/- SEM of 3 independent experiments). H Immunofluorescent analysis of the rate of double strand break repair marked by comparison of gammaH2AX foci marked breaks, homologous recombination RAD51 foci and 53BP1 foci as a marker for switch to non-homologous end joining in BT549 sensitive cells. I Immunofluorescent analysis of the rate of double strand break repair marked by comparison of gammaH2AX foci marked breaks, homologous recombination RAD51 foci and 53BP1 foci as a marker for switch to non-homologous end joining in BT549 resistant cells.

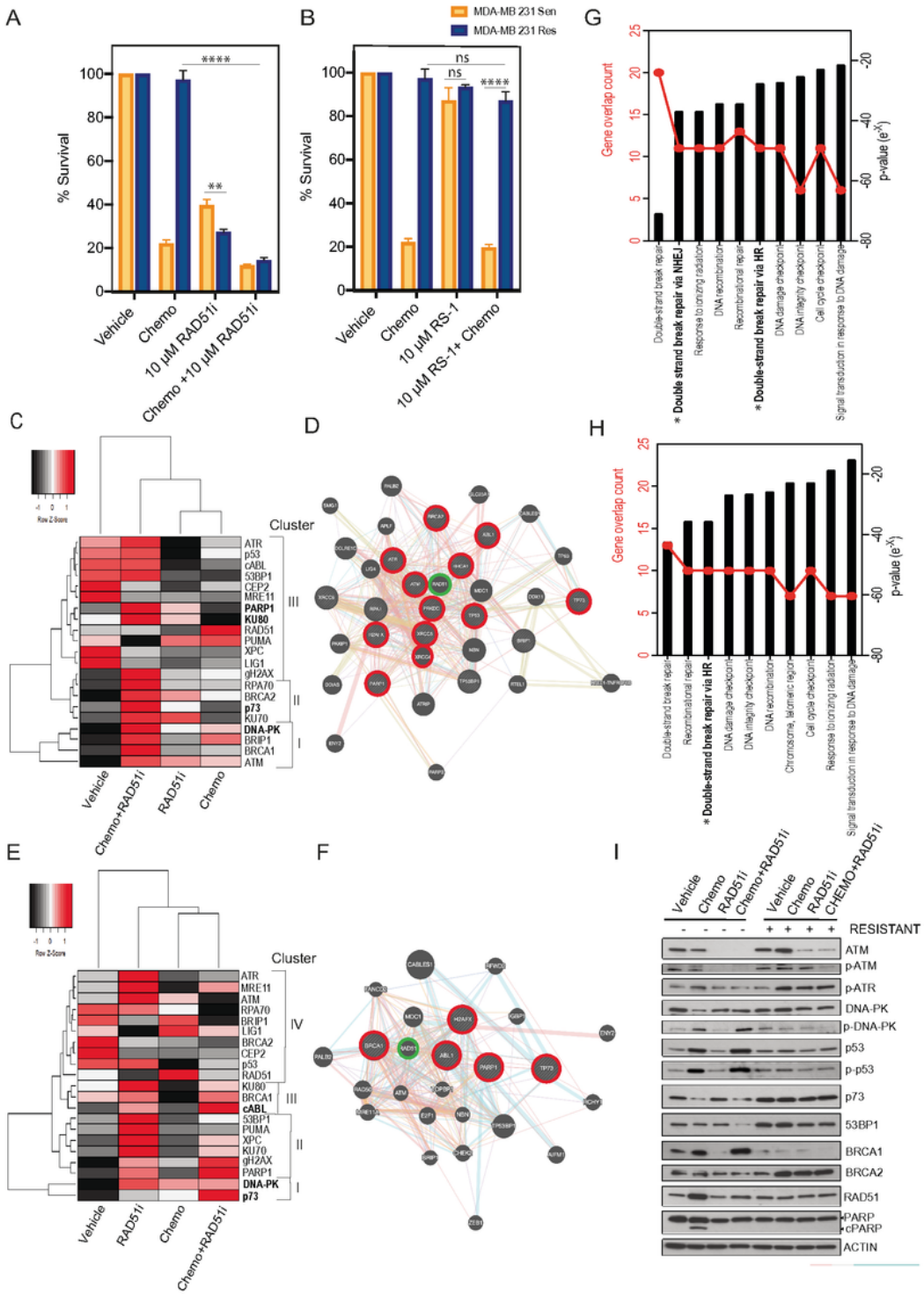

Figure 3

Sensitization of chemoresistant cells by targeting RAD51 and homologous recombination. A Metabolism assay targeting homologous recombination with a RAD51 inhibitor (****p<0.00001, **p<0.001 paired student t-test, +/- SEM of 3 independent experiments). B Metabolism assay targeting homologous recombination with a RAD51 stabilizer (****p<0.00001 paired student t-test, +/- SEM of 3 independent experiments). C Gene clustering of qPCR gene expression analysis of MDA-MB-231 sensitive cells

response to chemotherapy alone and in combination (Z-score -2 to +2 per gene across 4 conditions). D Functional interaction networks distances based on physical, colocalization and coexpression values. Key gene nodes of high expression after treated with chemotherapy and RAD51i are highlighted in red. RAD51 highlighted in green. Connectors, physical interactions (pink lines) and outliers joined by pathway association (blue lines). E Gene clustering of qPCR gene expression analysis of MDA-MB-231 resistant cells response to chemotherapy alone and in combination (Z-score -2 to +2 per gene across 4 conditions). F Functional interaction networks distances based on physical (pink lines), colocalization (blue lines) and coexpression values (purple lines). Key gene nodes of high expression after treated with chemotherapy and RAD51i are highlighted in red. RAD51 highlighted in green. Connectors, physical interactions (pink lines) and outliers joined by pathway association (blue lines). G Molecular signatures Database pathway analysis using curated gene set comparing response to chemotherapy and RAD51i in MDA-MB-231 SENS cells. H Molecular signatures Database pathway analysis using curated gene set comparing response to chemotherapy and RAD51i in MDA-MB-231 RES cells. I Protein expression analysis of MDA-MB-231 resistant and sensitive cells response to chemotherapy alone and in combination.

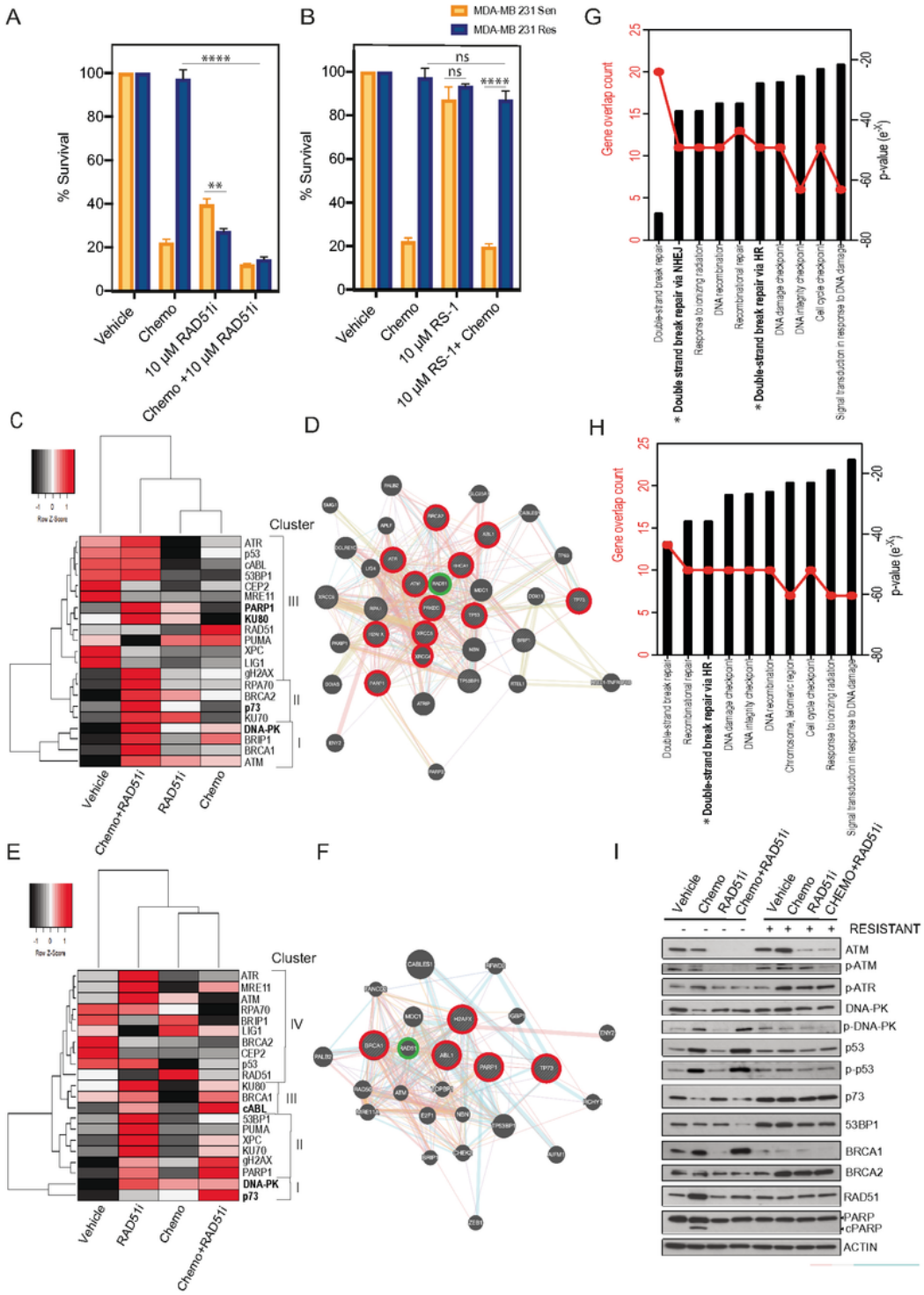

Figure 3

Sensitization of chemoresistant cells by targeting RAD51 and homologous recombination. A Metabolism assay targeting homologous recombination with a RAD51 inhibitor (****p<0.00001, **p<0.001 paired student t-test, +/- SEM of 3 independent experiments). B Metabolism assay targeting homologous recombination with a RAD51 stabilizer (****p<0.00001 paired student t-test, +/- SEM of 3 independent experiments). C Gene clustering of qPCR gene expression analysis of MDA-MB-231 sensitive cells

response to chemotherapy alone and in combination (Z-score -2 to +2 per gene across 4 conditions). D Functional interaction networks distances based on physical, colocalization and coexpression values. Key gene nodes of high expression after treated with chemotherapy and RAD51i are highlighted in red. RAD51 highlighted in green. Connectors, physical interactions (pink lines) and outliers joined by pathway association (blue lines). E Gene clustering of qPCR gene expression analysis of MDA-MB-231 resistant cells response to chemotherapy alone and in combination (Z-score -2 to +2 per gene across 4 conditions). F Functional interaction networks distances based on physical (pink lines), colocalization (blue lines) and coexpression values (purple lines). Key gene nodes of high expression after treated with chemotherapy and RAD51i are highlighted in red. RAD51 highlighted in green. Connectors, physical interactions (pink lines) and outliers joined by pathway association (blue lines). G Molecular signatures Database pathway analysis using curated gene set comparing response to chemotherapy and RAD51i in MDA-MB-231 SENS cells. H Molecular signatures Database pathway analysis using curated gene set comparing response to chemotherapy and RAD51i in MDA-MB-231 RES cells. I Protein expression analysis of MDA-MB-231 resistant and sensitive cells response to chemotherapy alone and in combination.

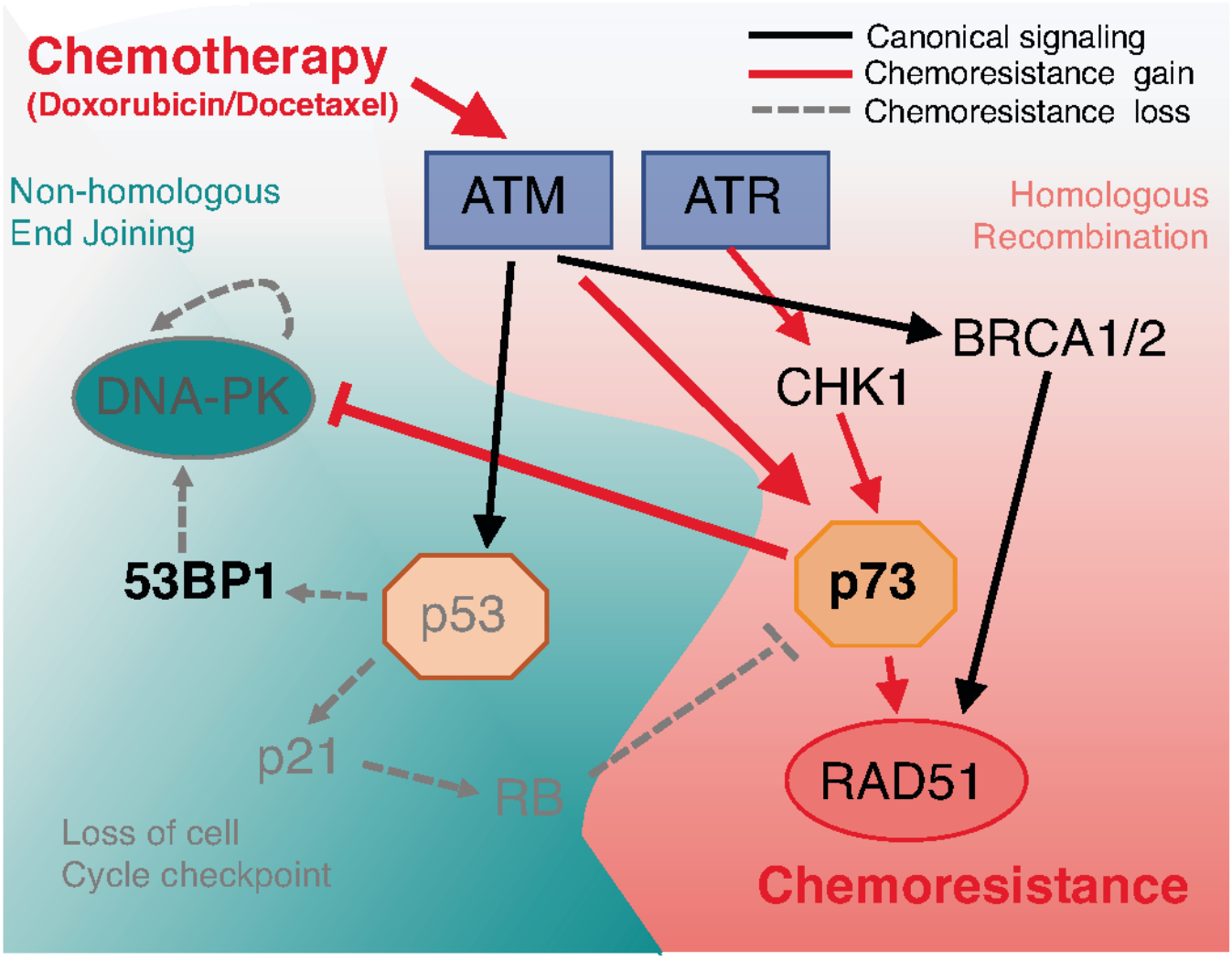

Figure 4

Pathway analysis under treatment conditions and resistance associated with induction of chemoresistance. Schematic diagram of chemoresistance signaling based on functional gene analysis and gene expression profiling observed in TNBC adapted cell lines.

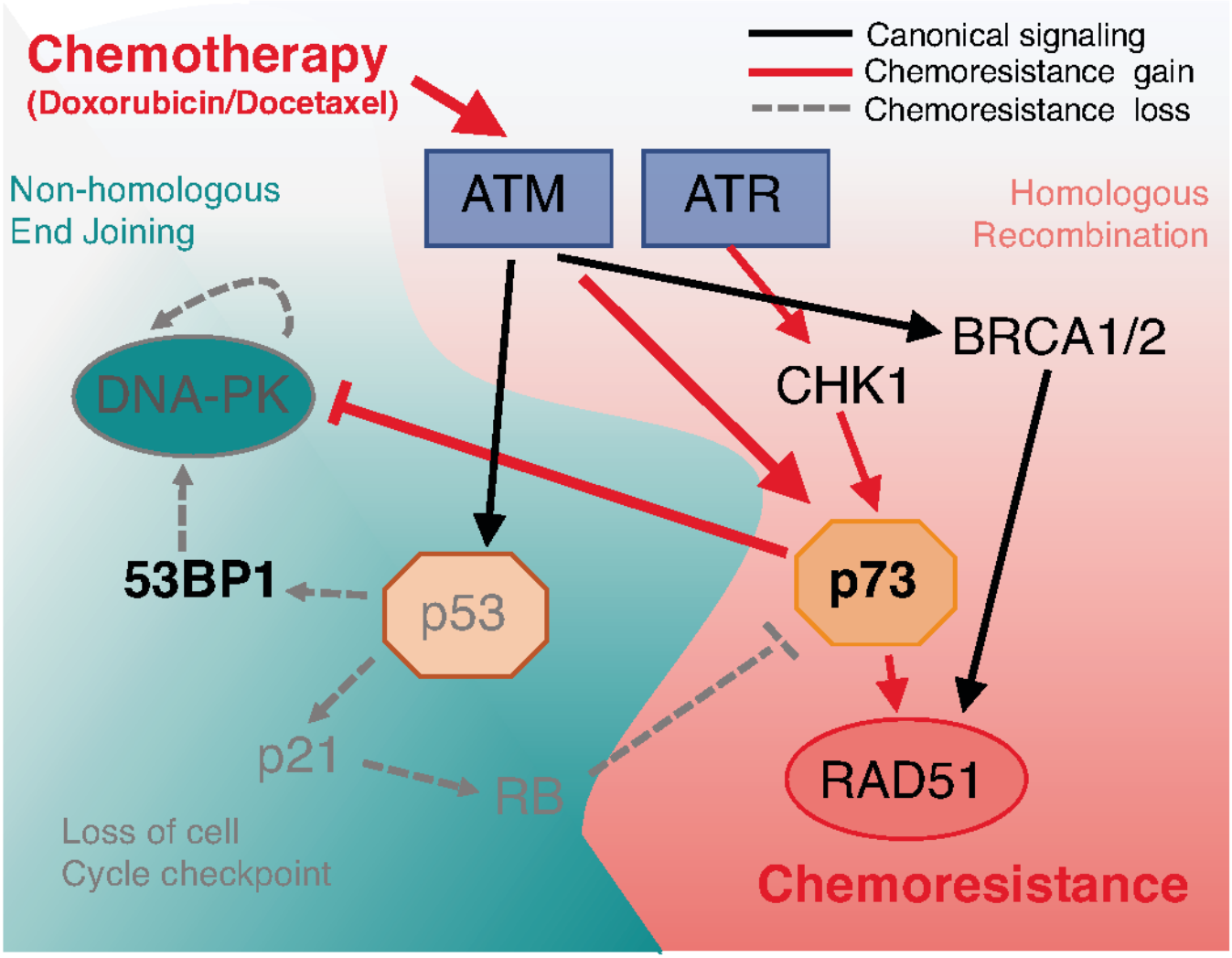

Figure 4

Pathway analysis under treatment conditions and resistance associated with induction of chemoresistance. Schematic diagram of chemoresistance signaling based on functional gene analysis and gene expression profiling observed in TNBC adapted cell lines.

Supplementary Files

This is a list of supplementary files associated with this preprint. Click to download.

- WiegmansWardShortSupplementaryfiles.pdf
- WiegmansWardShortSupplementaryfiles.pdf